Geoderma 262 (2016) 294–305

Contents lists available at ScienceDirect

Geoderma

journal homepage: www.elsevier.com/locate/geoderma

On the spatial variability of soil hydraulic properties in a Holocene coastal farmland

James Bevington [a,b,*], Davide Piragnolo [b], Pietro Teatini [c], George Vellidis [d], Francesco Morari [b]

[a] College of Engineering, University of Georgia, Athens, GA 30602, United States
[b] Dipartimento Agronomia Animali Alimenti Risorse Naturali e Ambiente, Agripolis, Universitá Di Padova, Viale Dell'Università, 16 35020, Legnaro, Pd, Italy
[c] Dipartimento di Ingegneria Civile, Edile e Ambientale, Universitá Di Padova, Via Marzolo, 9-35131 Padova, Italy
[d] Department of Crop and Soil Sciences, University of Georgia, Tifton, GA 31793, United States

ARTICLE INFO

Article history:
Received 16 October 2014
Received in revised form 30 June 2015
Accepted 16 August 2015

Keywords:
Spatial variability
Factorial kriging analysis
Water retention curve
van Genuchten model
Unsaturated hydraulic conductivity
Mualem model
Pedotransfer function

ABSTRACT

Understanding water movement in the vadose zone is critical for accurate climate and crop modeling, precision agriculture, soil–atmosphere gas exchanges, and contamination mitigation. A major reason for the difficulty of performing effective hydraulic measurements is because they are scale dependent due to the inherent heterogeneity of the soil. A better understanding of the spatial variability and underlying processes responsible for this variability could lead to a more accurate modeling. The goal of this study is to investigate the scale dependencies of soil hydraulic properties. Factorial kriging analysis (FKA) is a geostatistical technique which identifies scale dependent spatial relationships and common sources of variability. FKA was applied on a number of soil properties acquired from samples collected at 4 depths ranging from 8 to 68 cm in a 20.8 ha field in the Po River delta. The farmland is characterized by the presence of paleo-channel structures and highly heterogeneous soil. Texture, bulk density, K_s (saturated hydraulic conductivity), and the van Genuchten–Mualem parameters α (inverse of air entry), n (shape parameter), θ_r (residual water content), and θ_s (saturated water content) were included in the analysis. Two nested spherical models with ranges around 105 m and 235 m plus nugget fit the experimental variograms and cross-variograms best. Regionalized correlation coefficients and regionalized PCA revealed many strong, scale dependent relationships which were not obvious from descriptive statistics, such as the effect of interaction between texture and bulk density on n and K_s, and the stronger influence of bulk density than texture on K_s. The first principal components (PCs) of the regionalized PCA explained the majority of the variability and the second PCs were rarely informative. The spatial distributions of the first PCs resembled bulk density at short scale and the paleo-channels and texture at long scale. The decoupling of bulk density and texture is likely caused by differences in soil structure. The influence of the short scale PCs is greater than the long scale PCs near the surface but becomes less important as depth increases. This suggests that depth plays an important role and should be considered more often in spatial analysis.

1. Introduction

The vadose zone is of utmost importance in solving some of today's most challenging environmental issues. In particular, this zone is an integral part of the hydrological cycle and the interface between groundwater, vegetation, and atmospheric interactions. Water movement in the vadose zone differs greatly from water movement in other systems. Though much research on the complex interactions of soil and water movement has been completed, there is much progress to be made (Vereecken et al., 2010). Unsaturated water retention curves (WRCs) and hydraulic conductivity curves (UHCs) are most often described by the van Genuchten (1980) and Mualem (1976). Several studies have concluded that lab measurements differ from field measurements of the hydraulic parameters of the WRC and UHC (Wierenga et al., 1991; Mallants et al., 1997b). Spatial heterogeneity is suggested as the primary source of error. In particular, Mallants et al. (1997b) showed this to be true for measurements of saturated hydraulic conductivity (K_s). The variance of the K_s measurements decreases as sample volume increases, likely due to the existence of macropores and preferential flow paths. These local variations in soil structure initiate a predominant short-range autocorrelation of K_s. In addition, deterministic components related with pedogenetic processes (e.g. topography) affect K_s at larger scale of investigations (Zimmermann et al., 2013).

Abbreviations: BD, bulk density; ECa, apparent electrical conductivity; FKA, factorial kriging analysis; K_s, saturated conductivity; l, connectivity and tortuosity parameter; n, shape parameter; NDVI, Normalized Difference Vegetation Index; PCA, principal component analysis; PTF, pedotransfer function; SOC, soil organic carbon; UHC, unsaturated hydraulic conductivity curve; WRC, water retention curve; α, inverse of air entry; θ_r, residual water content; θ_s, saturated water content.

* Corresponding author.
E-mail address: jbevingt@gmail.com (J. Bevington).

http://dx.doi.org/10.1016/j.geoderma.2015.08.025
0016-7061/

Several studies have evaluated short scale variability (<25 m) of hydraulic parameters (Ciollaro and Romano, 1995; Mallants et al., 1997a; Hammel et al., 1999; Russo and Jury, 1987; Deurer and Duijnisveld, 2000), while most larger scale studies have focused on water content (θ) instead of hydraulic parameters (Botros et al., 2009; Bocchi et al., 2000; Goulard and Voltz, 1992; Voltz and Goulard, 1994). Spatial cross-correlation of hydraulic parameters has been investigated at short scale (Ünlü et al., 1990; Vauclin et al., 1994; Mallants et al., 1996; Mertens et al., 2002; Greminger et al., 1985). Using standard geostatistical interpolation methods (i.e. ordinary kriging and indicator kriging), Saito et al. (2009) compared the performances of two interpolation approaches to estimate the spatial distribution of UHC parameters of a 25 × 6 m domain and found that usually spatial correlation was <5 m. Moreover the existence of soil horizons resulted in a poor spatial correlation of parameters in the vertical direction.

Few studies have evaluated large scale spatial variability of hydraulic parameters.

Development of pedotransfer functions (PTFs) to predict hydraulic parameters from soil properties is an active area of research. These studies often incorporate advanced multivariate statistical techniques to build their prediction models. Inclusion of new and different explanatory variables is an active thrust in the field (Vereecken et al., 2010). Doussan and Ruy (2009) used apparent soil electrical conductivity (ECa) to predict UHC. Moreover, electrical surveys can also hold tremendous information about the spatial variability of soil (Corwin and Lesch, 2005).

On a 28.6 ha hill catchment, Herbst et al. (2006) applied coregionalization geostatistical methods (e.g. regression kriging model) using geomorphometric attributes (e.g. terrain slope and elevation) as co-variables. Strong effects of soil heterogeneity with depth on UHC parameters have been revealed by the authors.

The major drawback to measuring unsaturated hydraulic parameters is the time and cost involved and ideally would be reserved for cases when accuracy takes priority, e.g. shrink-swell studies. PTFs are best applied when accuracy can be sacrificed in exchange for sample quantity, e.g. when studying water movement of a field or catchment. A PTF that is valid for a large area is unlikely to model small scale phenomena well because of the difficulty in measuring many samples results in low sample density (Vereecken et al., 2010). Applications of downscaling to these widely applicable PTFs could benefit from knowledge of the spatial structure of the variables involved. Regardless of the PTFs use, development of PTFs could benefit from a deeper understanding of causal processes and new insight into relationships between soil variables and hydraulic parameters.

Factorial kriging analysis (FKA) is a geostatistical technique which dissects relationships based on scale dependencies (Groovaerts, 1998). At each scale, relationships are examined independent of the variability from relationships of other scales and common sources of variance in the spatial distributions identified. Sollitto et al. (2010) and Nanos and Martín (2012) were able to distinguish anthropogenic from natural sources of variation in trace elements typically associated with pollution. Dobermann et al. (1995) used FKA to investigate the relationships between soil chemistry, leaching, and hillslope position. Bocchi et al. (2000) applied FKA to soil properties and water content at several potentials. They explored the relationships between soil properties and water retention at different potentials and identified the effects of manure spreading on water retention. To the authors' knowledge, Biswas and Si (2009) is the only published use of FKA in conjunction with hydraulic parameters and soil properties. They studied a 384 m 1D transect in an area characterized by glacio-fluvial and fluvial lacustrine derived sandy loams. While they did explore novel relationships between hydraulic parameters, texture, bulk density and SOC, they were not able to investigate effects at scales larger than 200 m or identify an underlying process for the spatial distributions. Thus, relationships between soil properties and hydraulic parameters at larger scales remain uninvestigated and little scientific literature is available describing efforts to understand the underlying processes responsible for the patterns of variability seen in soil and hydraulic parameters.

This study will apply FKA to a field with a highly heterogeneous geomorphology at the southern margin of the Venice Lagoon, Italy, to investigate the scale dependencies of relationships between soil properties and hydraulic properties.

We hypothesized that 1) soil properties and hydraulic properties were affected by the same underlying processes and 2) that the relationships between soil properties and hydraulic properties are dependent on scale. The specific objectives of this study are to explore field scale spatial relationships between hydraulic parameters and soil physical properties and identify underlying processes responsible for spatial distributions found in the study. After a short description of the study area from hydrologic and geomorphologic points of view, the collected datasets and the geostatistical techniques used for their processing are described. Then, the results are presented highlighting the depth-dependent behavior of the spatial relationships between the soil physical and hydraulic properties with primary and secondary variables. A discussion session and conclusions close the paper.

2. Material and methods

2.1. Study site description

The study site is a 20.8 ha field located on the southern margin of the Venice Lagoon (Fig. 1). This area was reclaimed from the lagoon by the construction of levees between 1892 and 1967 (Gambolati et al., 2006). A pumping station and a dense network of ditches control the depth to the water table, which is generally maintained at ca. 0.6 m during the summer season in order to promote sub-irrigation. On the northern edge are the Morto Canal, Bacchiglione River, Brenta River, and the Venice Lagoon. All of the canals and the majority of the river courses are not natural as the rivers were diverted here at various times in the past. During construction of the Morto Canal, soil was placed on the northern edge of the field burying the original surface. Because of its reclaimed origin, soil shows a high variability in terms of texture, pH, salinity, and presence of organic horizons, which can be superficial as well as buried at deeper depth. Two main soil typologies can be identified according to USDA (1998). In the northern part, along the Morto Canal, soils are Fluvaquentic Endoaquepts fine-silty, mixed, calcareous, mesic, and in the southern part Typic Sulfisaprists euic, mesic. Furthermore, there are well preserved sandy paleo-river channels which cut through the field. These artifacts are related to the geomorphological evolution of this coastal area during the Holocene. In recent years, the field has been continuously used to grow corn (*Zea mais* L.) and is plowed to a depth of approximately 0.30 m.

2.2. Soil sampling and primary variables

A set of 123 sampling locations were selected in the study area using an apparent electrical conductivity (EC_a) survey and simulated annealing algorithm to account for the maximum amount of variability in the field while maintaining spatial coverage. Further details are described in Scudiero et al. (2011). Undisturbed samples were taken at 50 out of the 123 locations in October 2010 using a hydraulic core sampler. At each undisturbed location, core samples (7.2 cm diameter, 6 cm height) were removed at four depths: 0.05–0.11 m, 0.25–0.31 m, 0.45–0.51 m, and 0.65–0.71 m, referred to nominally according to their midpoint depth: 8 cm, 28 cm, 48 cm and 68 cm. These depths were chosen to provide even coverage of the approximately 1 m vadose zone.

Hydraulic measurements were made on 164 undisturbed cores. Although a higher number of tests should be preferable from a geostatistical point of view, the complexity of the testing procedure makes this number significant for spatial analyses of unsaturated hydraulic properties. Saturated hydraulic conductivity (K_s) was measured using a laboratory permeameter with ascendant water flow

(Eijkelkamp, Giesbeek, The Netherlands). Unsaturated hydraulic conductivity and retention curves were determined by applying the Wind method (Dane and Topp, 1994) using the Ku-pF Apparatus DT 04-01 (Umwelt-Geräte-Technik GmbH, Müncheberg, Germany). HYDRUS 1D v4.12 (Simunek et al., 2008) was applied to invert Richards' equation and calculate van Genuchten and Mualem parameters:

$$S_e = \frac{\theta(h) - \theta_r}{\theta_s - \theta_r} = \frac{1}{\left(1 + |\alpha h^n|\right)^m}$$

and

$$K(\theta) = K_s S_e^l \left[1 - \left(1 - S_e^{1/m}\right)^m\right]^2$$

where S_e is the effective saturation, l is the connectivity and tortuosity parameter, θ_r and θ_s are the residual and saturated water content (cm cm^{-1}), α (L^{-1}), n and m ($m = 1 - 1/n$) are empirical parameters, and K_s is the saturated hydraulic conductivity (cm d^{-1}).

Soil texture was measured using a Mastersizer 2000 (Malvern Instruments Ltd, Great Malvern, UK) while soil organic carbon (SOC) was measured using a vario MACRO elemental analyzer device in CNS mode (Elementar, Hanau, Germany).

2.3. Secondary variables

Exhaustive datasets are useful to geostatistical studies when used as secondary variables and can greatly improve the prediction of primary variables (Wackernagel, 2003). For this study, four data sets were collected, namely ECa at 0–0.75 m (ECa075) and 0–1.5 m (ECa150) depths, land elevation, and the inverse of bare soil reflectance as measured with the Normalized Difference Vegetation Index (NDVI). ECa datasets were collected in April 2011 using a CMD-1 frequency-domain electric induction sensor (GF Instruments, Brno, Czech Republic). The CMD-1 only collects one depth at a time because it must be reconfigured for different depths. The data logger collects two measurements at each point; all values at the same location were averaged together to have one representative value for the point. For ECa075, a number of 18,053 measurements were collected at 9017 locations and 20,471 ECa150 measurements were collected at 10,221 locations. Elevation was measured in February 2012 using a Trimble FM 1000 CNH GPS receiver with real time kinematic (RTK) differential correction (Trimble Navigation Ltd., Sunnyvale, CA, USA) at 1564 locations. Bare soil NDVI was measured in March 2012 using an APS1-CropCircle (Holland Scientific, Lincoln, NE, USA) at 10,214 locations. This sensor uses light reflectance at 590 nm (VIS) and 880 nm (NIR) to calculate NDVI using NDVI = (NIR − VIS) / (NIR + VIS) (Rouse et al., 1973). Each dataset was transformed, de-trended and interpolated using ordinary kriging to a 1 m resolution grid of 550 by 750 nodes using the approaches described below. Interpolated values at the grid nodes were exported for a principal component analysis (PCA). The loading of each node on principal component 1 (F1) was then used as a secondary variable in the geostatistical study.

2.4. Spatial statistics

Each depth was treated as an independent dataset to add independent observations of the spatial distributions and add strength to the spatial analysis. It is well documented in the literature that hydraulic parameters tend to not have normal distributions (Mallants et al., 1996, 1997b; Botros et al., 2009). Though it is not an explicit requirement of kriging, extreme distributions may yield unreliable results (Alary and Demougeot-Renard, 2010). For this reason, all variables were transformed using a Hermitian transformation algorithm (Wackernagel, 2003). The transformed variables are indicated with a′. After transformation, all variables were de-trended by fitting a constant, first or second order polynomial model to the data to satisfy the requirement of stationarity. Quality of fit was evaluated by calculating the standard deviation of the residuals. The model that produced the least variance in the residuals was selected. The four depths were treated as independent data sets.

2.5. Variography

Experimental variograms and cross-covariograms were calculated. Because of the semi-discontinuous interface between paleo-channels

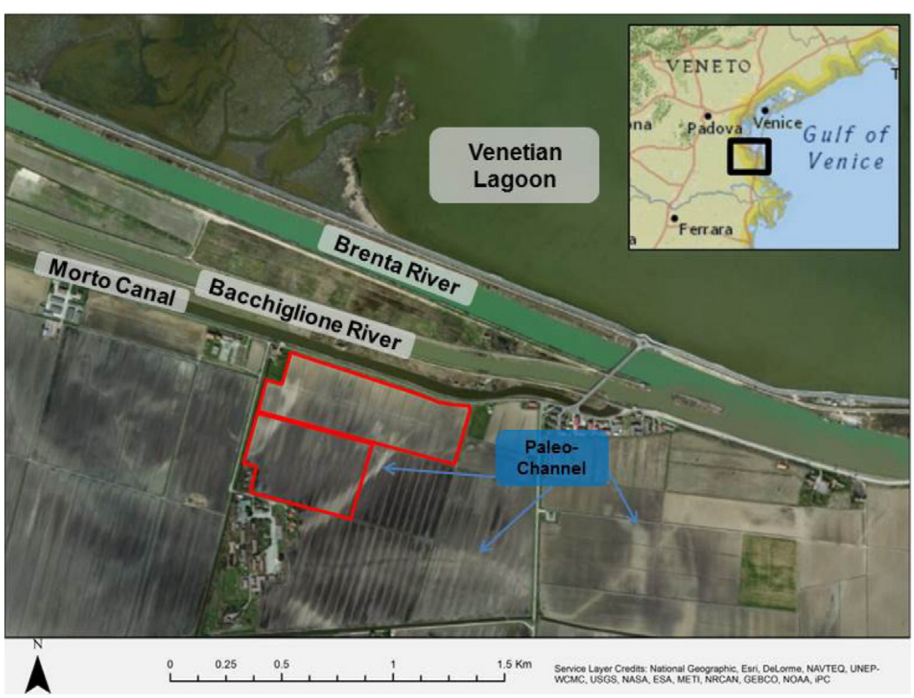

Fig. 1. Map of the study site which is located on the southern edge of the Venice Lagoon, Italy. The red rectangles bound the study site. The site is crossed by paleo-channels (marked in blue) which are clearly visible in the aerial photography.

Table 1
Summary statistics of primary variables.

	Obs	Mean	Median	Min	Max	Std. dev	CV	Skew	Kurt
BD (g/cm^3)	166	0.900	0.978	0.139	1.521	0.356	39.5	−0.60	−0.54
SOC (%)	128	10.04	7.81	0.10	26.99	6.86	68.3	0.58	−0.75
Clay (%)	163	15.73	15.06	0.85	34.26	8.25	52.4	0.38	−0.78
Sand (%)	163	45.39	43.78	12.95	92.09	18.70	41.2	0.37	−0.49
Silt (%)	163	38.87	40.46	7.06	62.51	11.45	29.4	−0.74	0.07
K_s (cm/d)	164	243.16	101.04	0.18	2630.10	405.24	166.7	3.89	18.43
l	164	−1.007	0.001	−19.496	6.201	2.774	−275.3	−2.90	13.70
α (1/cm)	164	0.046	0.032	0.003	0.184	0.036	77.9	1.36	1.47
n	164	1.45	1.22	1.07	4.14	0.53	36.9	2.68	8.27
θ_r (cm^3/cm^3)	164	0.199	0.195	0.000	0.599	0.121	60.8	0.73	0.91
θ_s (cm^3/cm^3)	164	0.603	0.580	0.298	0.950	0.129	21.4	0.63	−0.13

and surrounding material and the arrangement of data locations, 1 to 2 points per depth were masked during this calculation if they contributed many high variance pairs at short distances. Lags having less than 5 pairs at the shortest lag distance, and variances higher than the next longer lag were removed from further analysis because they prevented model fitting. These points are prone to occur because the sample locations were specifically selected to oversample areas with high variability such as the sharp paleo-channel interfaces which differ from the variability found in the rest of the field.

Many models were fit to the experimental variograms and cross-covariograms, with experimental points that were weighted based on the number of pairs in the lag. Quality of fit was evaluated by calculating the sum of squared residuals, and using the Akaike criterion and Bayesian Information criterion which all tended to agree. The linear

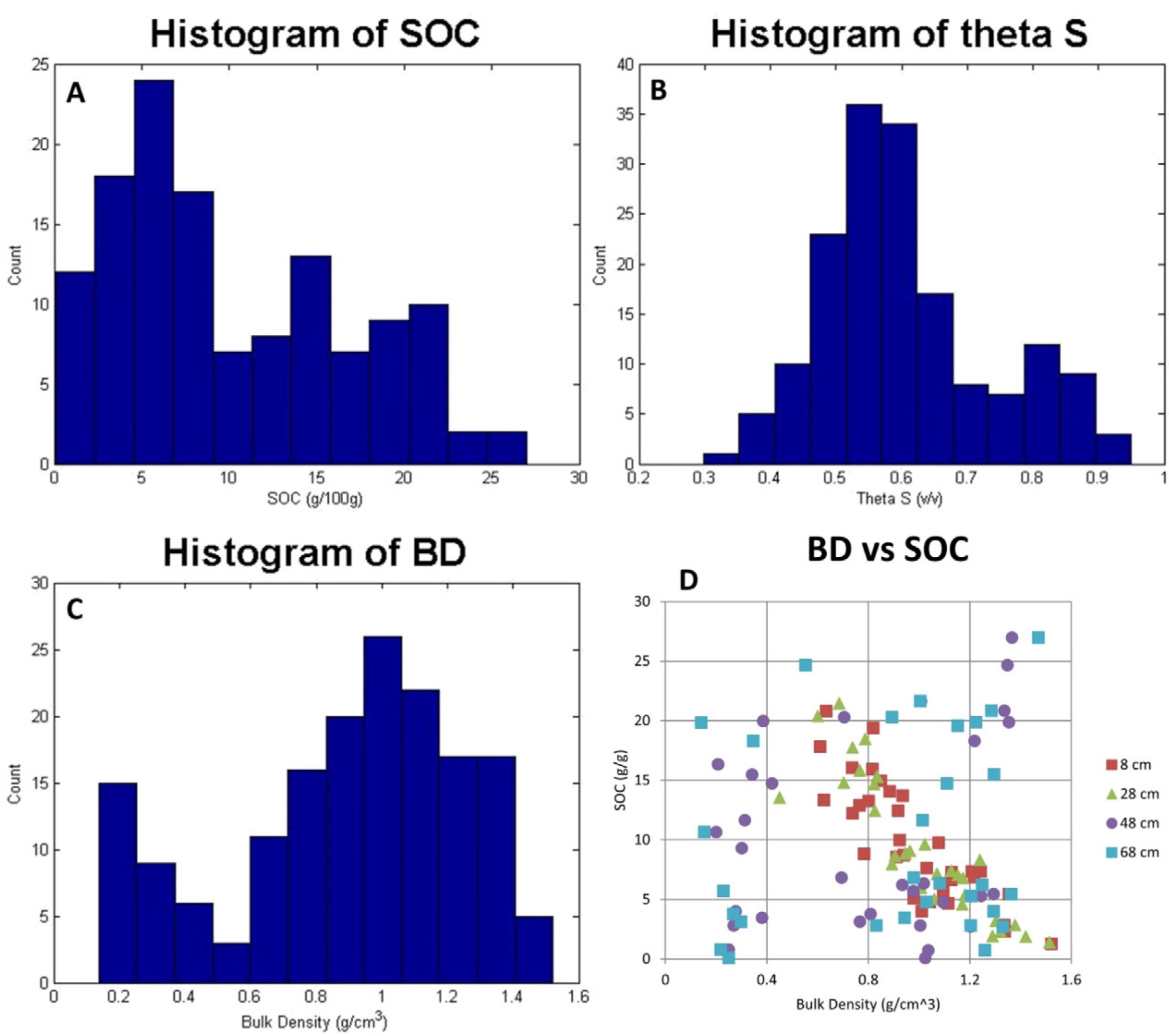

Fig. 2. A.) B.) C.) Histogram of SOC, θ_s, and bulk density, respectively. BD clearly has a bimodal distribution. This is also reflected in θ_s and to a lesser extent in SOC. D.) Scatter plot of SOC vs BD grouped according to depth. The 8 cm and 28 cm depths are characterized by a linear relationship while 48 cm and 68 cm are clustered.

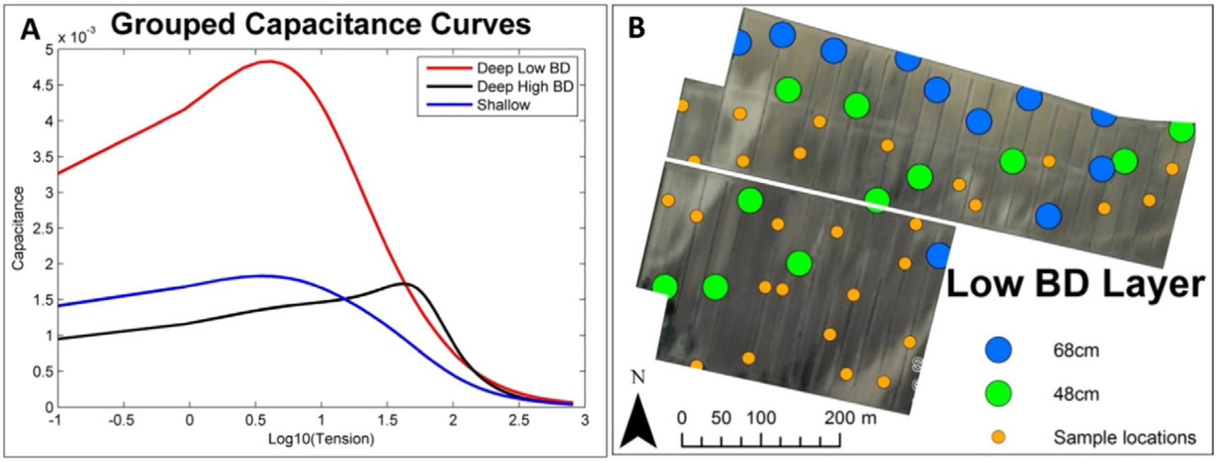

Fig. 3. A.) Capacitance curves reveal 3 different structural groups. Soils at shallow depths (8–28 cm) differ from soils at deeper depths (29–68 cm). Deep soils are further divided into high BD (BD > 0.5 g/cm^3) and low BD (BD < 0.5 g/cm^3) illustrating the relationship between BD and depth. B.) Map of the locations of low BD samples. The pattern reflects the field elevation pattern where the front portion of the field was buried during construction of the Morto Canal.

model of coregionalization LMC was used as a constraint in all multivariate models to ensure that the matrix of semivariances was negative semi-definite (Goovaerts, 1992). This model assumes that all variables are influenced by the same processes and therefore uses the same set of basic variogram structures for all variograms and cross-covariograms (Wackernagel, 2003). Nested models with up to three structures were tested (including nugget effect). Models were cross validated in two ways. First, a leave-one-out cross validation was preformed where only the collocated, secondary variable was known at the removed point. As an additional check, a second leave-one-out cross validation was preformed where all of the variables except the one being predicted were known at the removed point. Both cross validations were evaluated by calculating the correlation between the actual and predicted values for each variable.

2.6. Factorial kriging analysis

Because FKA has been thoroughly described in the literature (Goovaerts, 1992; Castrignanò et al., 2000; Chilés and Delfiner, 2012; Wackernagel, 2003), only a brief overview is given here. The approach consists of decomposing the set of original second-order random stationary variables $\{Z_i(\mathbf{x});\ i = 1,\ldots,N\}$ into a set of reciprocally orthogonal regionalized factors $\{Y_v^u(\mathbf{x});\ v = 1,\ldots,n;\ u = 1,\ldots,N_S\}$ where N_S is the number of spatial scales, through transformation coefficients a_{iv}^u, combining the spatial with the multivariate decomposition:

$$Z_i(\mathbf{x}) = \sum_{u=1}^{N_S}\sum_{v=1}^{n} a_{iv}^u Y_v^u(\mathbf{x}). \tag{1}$$

The three basic steps of FKA are as follows (Castrignanò et al., 2000):

1) Modeling the coregionalization of a set of variables, using the so-called linear model of coregionalization (LMC; Wackernagel, 2003), and estimating soil attributes by cokriging;
2) analyzing the correlation structure between the variables at the different spatial scales by applying principal component analysis (PCA);
3) cokriging specific factors at characteristic scales and mapping them.

The LMC, developed by Journel and Huijbregts (1978), assumes that all the studied variables are the result of the same independent processes, acting at different spatial scales u. The $N(N+1)/2$ simple and cross semivariograms of the N variables are modeled by a linear combination of N_S standardized semivariograms to unit sill, $g^u(\boldsymbol{h})$. Using the matrix notation, the LMC can be written as:

$$\boldsymbol{\Gamma}(h) = \sum_{u=1}^{N_S} \mathrm{B}^u g^u(\mathbf{h}) \tag{2}$$

where $\boldsymbol{\Gamma}(h) = [\gamma_{ij}(\mathbf{h})]$ is a symmetric matrix of order $N \times N$, whose diagonal and non-diagonal elements represent simple and cross semivariograms, respectively for lag h; $\boldsymbol{B}^u = [b^u{}_{ij}]$ is called coregionalization matrix and is a symmetric positive semi-definite matrix of the order $N \times N$ with real elements $b^u{}_{ij}$ at a specific spatial scale u. The model is authorized if the mathematical functions $g^u(\mathbf{h})$ are authorized semivariogram models. The mapped PCs visually show the sources of variance and can be interpreted to infer the underlying processes. Regionalized principal component analysis consists of decomposing each

Table 2
Correlation table of transformed variables calculated with casewise deletion of missing values.

	BD′	SOC′	Clay′	Sand′	Silt′	K_s′	l′	α′	n′	θ_r′	θ_s′
BD′											
SOC′	−0.14										
Clay′	−0.08	−0.18									
Sand′	0.13	0.23	**−0.94**								
Silt′	−0.19	−0.21	**0.82**	**−0.95**							
K_s′	**−0.36**	0.03	0.01	0.03	−0.06						
l′	−0.21	−0.03	−0.24	0.25	−0.24	**0.41**					
α′	**−0.51**	−0.02	0.25	−0.21	0.16	**0.59**	−0.09				
n′	0.18	0.13	**−0.72**	**0.7**	**−0.63**	−0.14	0.19	−0.22			
θ_r′	**−0.33**	0.06	−0.02	−0.03	0.11	−0.06	−0.04	0.28	0.25		
θ_s′	**−0.87**	0.12	0.25	**−0.32**	**0.37**	0.23	0.11	**0.37**	**−0.37**	**0.35**	

(N = 126) Bold font denotes significance of P < 0.001.

Table 3
Summary of spatial models.

Depth (nom.)	# of Vars[a]	Short[b](m)	Long[b] (m)	SSR[c]	L/S[d]
8	9	106.8	224.5	0.028	0.759
28	8	153.0	285.4	0.049	0.877
48	9	74.2	209.9	0.094	1.627
68	8	92.0	216.5	0.098	4.267

[a] # of Vars is the number of variables used in the spatial model.
[b] Short and long represent the short and long scale ranges for the spatial models respectively.
[c] SSR is the sum of squared residuals of the experimental data to the fitted model.
[d] L/S is the ratio of long to short scale Eigenvalues of the first PCs and represents a ratio of the variance represented by long scale processes to that of short scale processes.

Table 4
Leave-one-out cross validation with only secondary variable known.

Depth (nom.)	8	28	48	68
BD*	0.65	0.64	0.48	0.62
Sand*	0.39	0.36	0.47	0.52
Clay*	0.36	NA	0.48	NA
K_s*	0.22	0.31	0.33	0.43
α*	0.44	0.34	0.35	0.65
n*	0.24	0.39	0.42	0.62
θ_r*	0.30	0.22	0.07	0.12
θ_s*	0.64	0.55	0.47	0.72

Values are correlations between actual and predicted.

Table 5
Leave-one-out cross validation with all variables known.

Depth (nom.)	8	28	48	68
BD*	0.89	0.90	0.93	0.86
Sand*	0.88	0.39	0.90	0.65
Clay*	0.86	NA	0.91	NA
K_s*	0.60	0.65	0.66	0.60
α*	0.75	0.71	0.84	0.89
n*	0.78	0.76	0.73	0.73
θ_r*	0.76	0.78	0.64	0.54
θ_s*	0.91	0.78	0.93	0.84

Values are correlation between actual and predicted.

coregionalization matrix $\boldsymbol{B}^u$ into two other diagonal matrices: the matrix of eigenvectors and the matrix of eigenvalues for each spatial scale u through the matrix $\boldsymbol{A}^u$ of order $N \times N$ of the transformation coefficients a_{iv}^u (Wackernagel, 2003). The transformation coefficients a_{iv}^u in the matrix $\boldsymbol{A}^u$ correspond to the covariances between the original variables $Z_i(x)$ and the regionalized factors $Y_v^u(\mathbf{x})$. The behavior and relationships among variables at different spatial scales can be displayed by interpolating the regionalized factors $Y_v^u(\mathbf{x})$ using cokriging and mapping them. After a model was fitted, regionalized correlation coefficients were calculated from the respective sill values. Using the regionalized correlation matrices as input, a regionalized PCA was computed for each range as a normal PCA would be. Maps of each PC were made by interpolating the projection of the measured points on the PC of interest. Secondary data were incorporated in a multi-collocated cokriging scheme to improve accuracy of interpolation and therefore the map reliability.

All of the geostatistics were performed using ISATIS (Geovariances and Ecole des Mines de Paris, 2013). Some graphical and data processing tools from ArcMap 10.1 (ESRI, Redlands, CA, USA) and Matlab (MathWorks, Natick, MA) were also used.

3. Results and discussion

3.1. Descriptive statistics

For the most part the distributions of primary variables are not normal. In particular, l, K_s, and n have strongly asymmetric distributions with an absolute skewness higher than 2. The connectivity and tortuosity parameter l, is very near -1 on average (Table 1) confirming the results of Schaap and Leij (2000) which found that -1 was a better value for l than 0.5, the commonly used value (Mualem, 1976). Bulk density and θ_s have a bimodal distribution which is most obvious on the lower range of bulk density as seen in Fig. 2C. The contrasting nature of the soils, characterized by the presence of peaty horizons (Gambolati et al., 2006), could have influenced this behavior. If this is the reason, a similar bimodal distribution would be also expected for SOC. However, a visual inspection of the SOC histogram (Fig. 2) is inconclusive. A scatter plot of SOC vs BD (Fig. 2) reveals a clear negative relationship at the 8 cm and 28 cm depths, as usually observed (Loveland and Webb, 2003), but no trend or an unclear trend is observed at 48 cm and 68 cm depths. This shallower versus deeper grouping is common among many variables most likely because of the 30-cm depth plowing (Scudiero et al., 2013) that could have influenced the soil structure. Other authors have highlighted that the spatial distribution of hydraulic properties related to natural pedogenetic processes can be affected by anthropogenic activities at shallow depth (Herbst et al., 2006).

Another possible explanation for the bimodal BD distribution is soil structure. Structural information was not recorded on the soil samples but pore size distributions can be used as a substitute. A pore size distribution can be approximated by the capacitance function which is the derivative of the WRC curve (Radcliffe and Simunek, 2010). Grouping and averaging the capacitance curves by depth and bulk density (Fig. 3A) reveal three groups with differing structures.

All but one of the low BD samples (BD < 0.5 g/cm^3) are located at 48 cm and 68 cm. Fig. 3B reveals that these points are all near the northern edge and away from the paleo-channels. Because this front edge was filled in, deeper samples in this portion of the field will represent the original surface and will reflect properties of the original soils.

In order to add clarity to the analysis of relationships, the correlation matrix of Pearson correlation coefficients of the transformed variables was calculated using casewise deletion of missing values (Table 2). Bulk density is not correlated with texture, a finding that emphasizes the complex nature of the variable. Many of the well documented correlations among hydraulic variables are also observed, for instance α and K_s, BD and θ_s (Walczak et al., 2002; Botros et al., 2009; Mallants et al., 1996). One expected relationship that is not found is between texture and K_s.

3.2. Secondary variables

Apparent soil electrical conductivity and bare-soil NDVI spatial data displayed high variability across the study site. The ECa075 and ECa150 maps showed nearly identical spatial patterns, yet they differed in values and ranges. The ECa075 was characterized by an average (0.65 dS m^{-1}) lower than that of ECa150. The lowest ECa values were observed in the paleochannels, with minimum values equal to 0.12 and 0.31 dS m^{-1} for ECa075 and ECa150, respectively, recorded in the western paleochannel (low clay content, low SOC, and high BD). Conversely, the maximum ECa values (1.75 and 2.78 dS m^{-1} for ECa075 and ECa 150, respectively) were associated with saline loamy soils in the northern part of the study site. Bare-soil NDVI also varied greatly across the area, with a north–south gradient: in the northern part of the study site, where texture was finer, NDVI ranged between 0.148 and 0.242. The NDVI increased gradually southward reaching a maximum value of 0.418.

A PCA of the residuals of the four transformed data sets, ECa075, ECa150, elevation, and NDVI, offers a principal component (F1) which describes 80.1% of the variance in the data. Both ECa data sets contributed strongly on this component and land elevation to a lesser extent. Elevation contributed in an opposite direction to ECa on F1. NDVI did not significantly load on F1 but contributed strongly on principal component 2 (F2). Because only F1 is used in the subsequent analysis, NDVI does not add much to this study.

3.3. Spatial statistics

3.3.1. Variography

The best fit of the experimental variograms was obtained by a two-nested spherical model (Table 3). Fitting the linear model of coregionalization (LMC) becomes more difficult as the number N of variables is added to the analysis increases, since it requires $N(N+1)/2$ variograms. For this reason, only the most representative variables were selected. Sand and clay were used to represent texture, but clay was excluded for 8 cm and 68 cm depths. SOC at 8 cm and 28 cm depths followed the same patterns as BD and added little new information as expected because of the strong global correlation between these two parameters. At depths of 48 cm and 68 cm, SOC had a poor spatial structure characterized by high nugget effect and hence was removed from the analysis. F1 was used as a secondary variable for all depths except 8 cm where elevation was more informative. Over all, short ranges (short) tended to be around 105 m and long ranges (long) about 235 m. The leave-one-out cross validation where only the secondary variable is known illustrates that the models represent some individual variables only moderately well while others are represented much better (Table 4). However, given the large number of variables, this is to be expected. The second cross validation approach (Table 5) where all of the non-predicted variables are known results in much higher correlations. It is worth noting that, although a higher sample number would improve the results, the cross-validation presented in Tables 4 and 5 supports the validity of the results, also accounting for the complexity of the hydraulic analyses.

3.3.2. Regionalized relationships

The regionalized correlations show many strong relationships that were not obvious from the global correlations summarized in Table 2. Finding these trends reveals the benefit of including scale and autocorrelation in soil analysis. The variables in this section are the residuals from de-trending the transformed variables and are indicated with a*. In most cases, the primary variables had a strong correlation with the secondary variable for at least one range. This means that secondary variables hold relevant information to this study.

Sand* and n* have a very strong, positive relationship at long range; at short range, trends change with depth from strong positive at 8 cm and 28 cm to no correlation and negative correlation at 68 cm. This is interesting because sand′ and $n′$ were globally correlated (all depth considered together). Typically, variables that are globally correlated show the same relationships at all scales as the relationship is not necessarily scale dependent. In this case, at the depths where the correlation coefficients of sand* and n* are opposite, the influence of the short scale process is less than the influence of the long scale processes (Tables 6–9). Sand* and α* are negatively correlated throughout all ranges and depths, a finding opposite to many others (Biswas and Si, 2009; Li et al., 2006). The magnitude of the Sand* and α* relationships indicates that the nugget effect on these variables masks important information and reveals the advantage of investigating the effects of scale as globally, these two variables did not have a clear relationship.

Except for 8 cm long range (Table 6), α* and BD* have a strong, negative correlation. Biswas and Si (2009) also found a negative α and BD relationship. BD* and K_s* and Sand* and K_s* are mostly negatively correlated except for at 48 cm long scale (Table 8) and 68 cm short scale (Table 9). The relationships between BD* and K_s* are stronger than the relationships between texture* and K_s*, indicating a major role played by bulk density on K_s and explaining the oddly negative relationships observed between K_s and sand, in oppositions to many other findings (e.g. Jaynes and Tyler, 1984; Puckett et al., 1985).

At short scale, the BD* and K_s* relationship acts in the same direction as the BD* and n* relationship at some depths, but at others, they act in different directions. Whether or not they act in the same or a different direction appears to be related to the strength of the relationship between BD* and Sand*. If the BD* and Sand* relationship is strong, they act in opposite directions, if it is weak, they act in the same direction. This suggests that an interaction between texture and bulk density may influence relationships with these hydraulic parameters. Of all of the parameters, θ_r tends to have the least physical significance and is viewed by many researchers as a fitting parameter (Radcliffe and Simunek, 2010). Because of this, it added little to the analysis.

Many of the relationships are strong but variable with depth. This variability masks global trends and makes deciphering the processes

Table 6
Regionalized correlation coefficients at 8 cm depth.

	Elev*	BD*	Clay*	Sand*	K_s*	α*	n*	θ_r*	θ_s*
Elev*		**0.89**	−0.18	0.26	**−0.95**	−0.07	**0.51**	**−0.79**	**−0.74**
BD*	**0.77**		−0.01	0.02	**−0.88**	0.36	**0.56**	**−0.80**	**−0.65**
Clay*	−0.18	**−0.55**		**−0.99**	0.43	**0.66**	**−0.78**	**0.60**	**0.77**
Sand*	0.08	**0.53**	**−0.99**		−0.47	**−0.75**	**0.73**	**−0.59**	**−0.78**
K_s*	**−0.72**	**−0.86**	0.07	−0.08		0.12	**−0.75**	**0.93**	**0.90**
α*	**−0.83**	**−0.93**	**0.67**	**−0.61**	**0.66**		−0.12	0.05	0.32
n*	0.26	**0.57**	**−0.99**	**0.96**	−0.08	**−0.73**		**−0.93**	**−0.93**
θ_r*	0.00	−0.09	**0.83**	**−0.77**	−0.43	0.38	**−0.85**		**0.96**
θ_s*	**−0.70**	**−0.99**	**0.57**	**−0.57**	**0.86**	**0.90**	**−0.59**	0.08	

Bottom triangle is short range coefficients and top triangle is long range coefficients. Bold values denote statistical significance (P = 0.0005) as calculated by an F-test.

Table 7
Regionalized correlation coefficients at 28 cm depth.

	F1	BD*	Sand*	K_s*	α*	n*	θ_r*	θ_s*
F1		**−1.00**	**−0.13**	**0.34**	**0.60**	**−0.31**	**0.44**	**0.86**
BD*	**−1.00**		0.17	−0.37	**−0.62**	0.35	−0.39	**−0.85**
Sand*	**−1.00**	**0.99**		**−0.92**	**−0.75**	**0.94**	**0.78**	−0.14
K_s*	**0.79**	**−0.81**	**−0.74**		**0.94**	**−1.00**	−0.48	0.49
α*	**0.99**	**−1.00**	**−0.98**	**0.85**		**−0.93**	−0.18	**0.75**
n*	**−0.80**	**0.82**	**0.75**	**−1.00**	**−0.86**		0.53	−0.45
θ_r*	**0.83**	**−0.84**	**−0.78**	**1.00**	**0.88**	**−1.00**		0.51
θ_s*	**0.95**	**−0.96**	**−0.92**	**0.94**	**0.98**	**−0.94**	**0.96**	

Bottom triangle is short range coefficients and top triangle is long range coefficients. Bold values denote statistical significance (P = 0.0005) as calculated by an F-test.

Table 8
Regionalized correlation coefficients at 48 cm depth.

	F1	BD*	Clay*	Sand*	K_s*	α*	n*	θ_r*	θ_s*
F1		**−0.57**	**0.70**	**−0.66**	−0.40	0.49	**−0.65**	−0.34	**0.57**
BD*	**−0.97**		**−0.67**	**0.62**	**0.54**	−0.33	**0.78**	0.05	**−0.96**
Clay*	−0.08	0.21		**−0.98**	−0.03	0.29	**−0.97**	**−0.76**	**0.68**
Sand*	−0.07	0.25	**0.78**		−0.10	−0.31	**0.97**	**0.78**	**−0.67**
K_s*	**0.55**	**−0.61**	0.17	−0.38		0.18	0.07	−0.48	−0.47
α*	**0.70**	**−0.77**	0.05	−0.40	**0.97**		−0.29	−0.10	0.23
n*	**0.97**	**−0.96**	0.06	−0.07	**0.71**	**0.83**		**0.64**	**−0.81**
θ_r*	**0.64**	**−0.63**	0.40	−0.08	**0.94**	**0.92**	**0.79**		−0.07
θ_s*	**0.99**	**−0.93**	−0.05	0.03	0.46	**0.61**	**0.93**	**0.59**	

Bottom triangle is short range coefficients and top triangle is long range coefficients. Bold values denote statistical significance (P = 0.0005) as calculated by an F-test.

Table 9
Regionalized correlation coefficients at 68 cm depth.

	F1	BD*	Sand*	K_s*	α*	n*	θ_r*	θ_s*
F1		−0.30	**−0.62**	0.03	0.36	−0.52	0.21	0.36
BD*	**−0.99**		**0.83**	**−0.96**	**−0.92**	**0.89**	0.16	**−0.99**
Sand*	**−0.82**	**0.89**		**−0.67**	**−0.95**	**0.99**	−0.36	**−0.89**
K_s*	**−0.72**	**0.80**	**0.99**		**0.84**	**−0.76**	−0.29	**0.93**
α*	0.09	−0.21	**−0.64**	**−0.76**		**−0.98**	0.23	**0.96**
n*	**0.93**	**−0.97**	**−0.97**	**−0.92**	0.44		−0.29	**−0.94**
θ_r*	**0.61**	**−0.70**	**−0.95**	**−0.99**	**0.84**	**0.85**		−0.05
θ_s*	**1.00**	**−1.00**	**−0.86**	**−0.76**	0.15	**0.96**	**0.66**	

Bottom triangle is short range coefficients and top triangle is long range coefficients. Bold values denote statistical significance (P = 0.0005) as calculated by an F-test.

Table 10
Regionalized PCA summary.

	Elev*	F1	BD*	Clay*	Sand*	K_s*	α*	n*	θ_r*	θ_s*	Eigen	% var
PC1S8	0.11	NA	0.44	−0.18	0.21	−0.30	−0.67	0.23	−0.07	−0.35	1.70	76.8
PC2S8	−0.11	NA	−0.19	−0.35	0.43	0.55	−0.05	0.42	−0.38	0.14	0.43	19.5
PC1L8	0.20	NA	0.22	−0.41	0.48	−0.20	−0.01	0.12	−0.40	−0.54	1.29	72.5
PC2L8	−0.34	NA	−0.58	−0.43	0.48	0.21	−0.02	−0.01	0.26	0.13	0.46	25.7
PC1S28	NA	−0.47	0.42	NA	0.11	−0.32	−0.44	0.25	−0.12	−0.47	1.95	94.4
PC2S28	NA	0.41	−0.32	NA	−0.14	−0.62	0.19	0.47	−0.20	−0.19	0.12	5.6
PC1L28	NA	0.75	−0.43	NA	−0.15	0.17	0.14	−0.17	0.14	0.38	1.71	61.0
PC2L28	NA	−0.17	0.07	NA	−0.65	0.35	0.15	−0.39	−0.49	−0.05	0.97	34.5
PC1S48	NA	0.31	−0.46	0.01	−0.02	0.48	0.43	0.08	0.36	0.38	2.39	78.1
PC2S48	NA	−0.33	0.41	0.08	−0.05	0.54	0.27	−0.04	0.30	−0.51	0.56	18.3
PC1L48	NA	0.46	−0.15	0.45	−0.48	−0.01	0.10	−0.52	−0.12	0.18	3.89	77.9
PC2L48	NA	0.81	−0.02	−0.20	0.28	−0.08	0.30	0.30	0.18	−0.01	0.62	12.5
PC1S68	NA	−0.48	0.50	NA	0.25	0.15	−0.08	−0.12	−0.54	−0.35	0.97	83.4
PC2S68	NA	−0.45	0.30	NA	−0.12	−0.14	0.33	−0.01	0.71	−0.26	0.19	16.6
PC1L68	NA	−0.32	0.36	NA	0.44	−0.22	−0.43	0.45	−0.04	−0.38	4.15	73.8
PC2L68	NA	−0.86	−0.25	NA	0.09	0.30	0.18	−0.03	−0.15	0.21	1.12	19.9

difficult. One source of inconsistency is associated with the bimodal distribution of bulk density. The different modes likely act in very different ways and as a consequence it is possible that studying them independently would be more informative. Similarly, Zimmermann et al. (2013) have found difficulties in detecting deterministic trends in Ks patterns because of the variability associated to the small-scale spatial variation. However, that analysis is beyond the scope of this study. While many relationships are explored here, the soil structure is one potentially revealing variable that is not addressed in this study. Texture and bulk density have very inconsistent relationships with hydraulic parameters (Weynants et al., 2009; Schaap and Bouten, 1996; Wösten et al., 2001) and are not well understood. Soil structure is likely to capture the interaction effects between texture and bulk density (David Radcliffe, personal communication) which may aid in deciphering these complex relationships. Soil structure has also been suggested as a potential predictor variable for PTF (Pachepsky et al., 2006; Li et al., 2006). At all depths and scales, the first PC explained the majority of the variance ranging from 94.4% to 61.0% (Table 10). The second PC

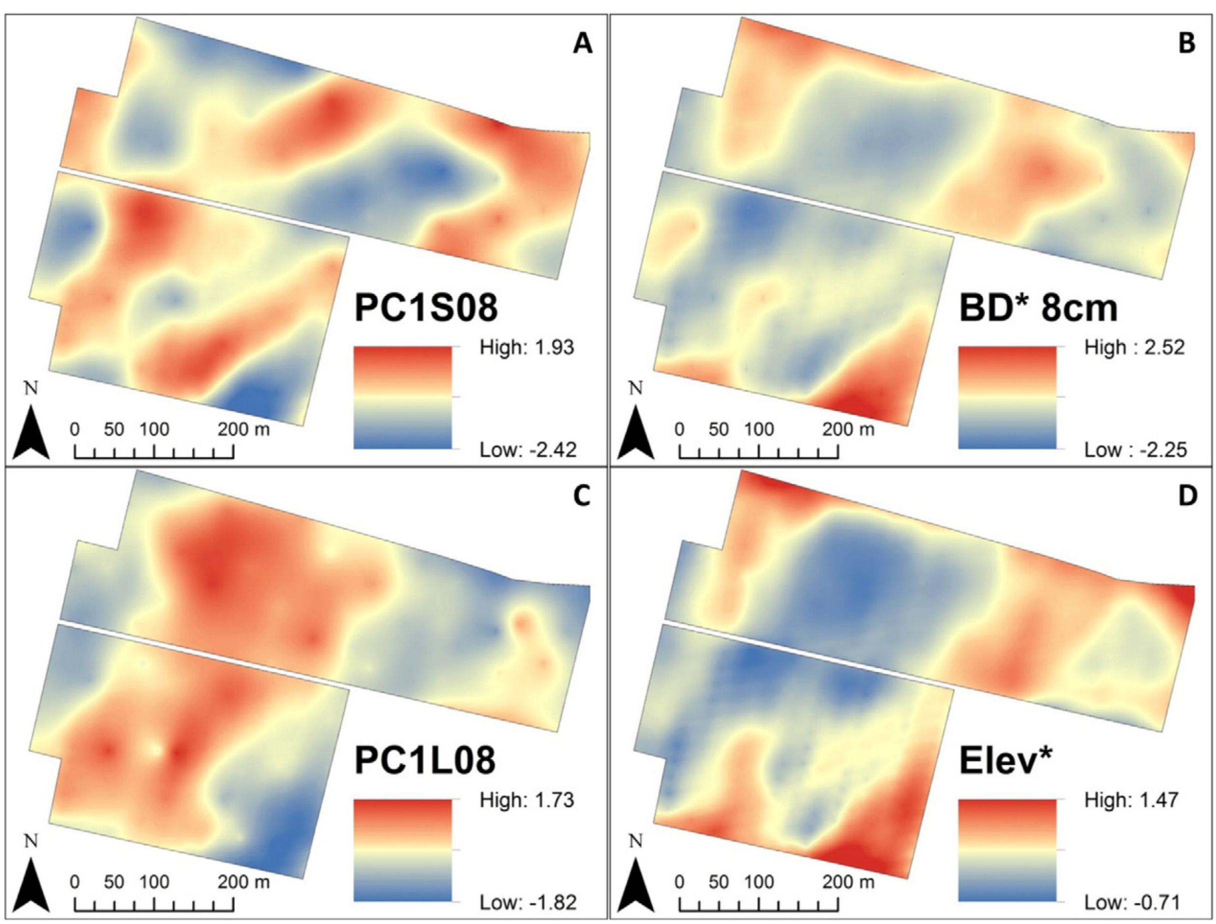

Fig. 4. Maps of retained PCs and their distribution counterparts at 8 cm depth. S1XX designates short range while S2XX designates long range. F1, F2, etc. designates the principal component in ranked order from most variance explained to least variance explained. Maps in the left column are FKA results and maps in the right column are the best physical match to the FKA maps based on visual assessment of the spatial distribution.

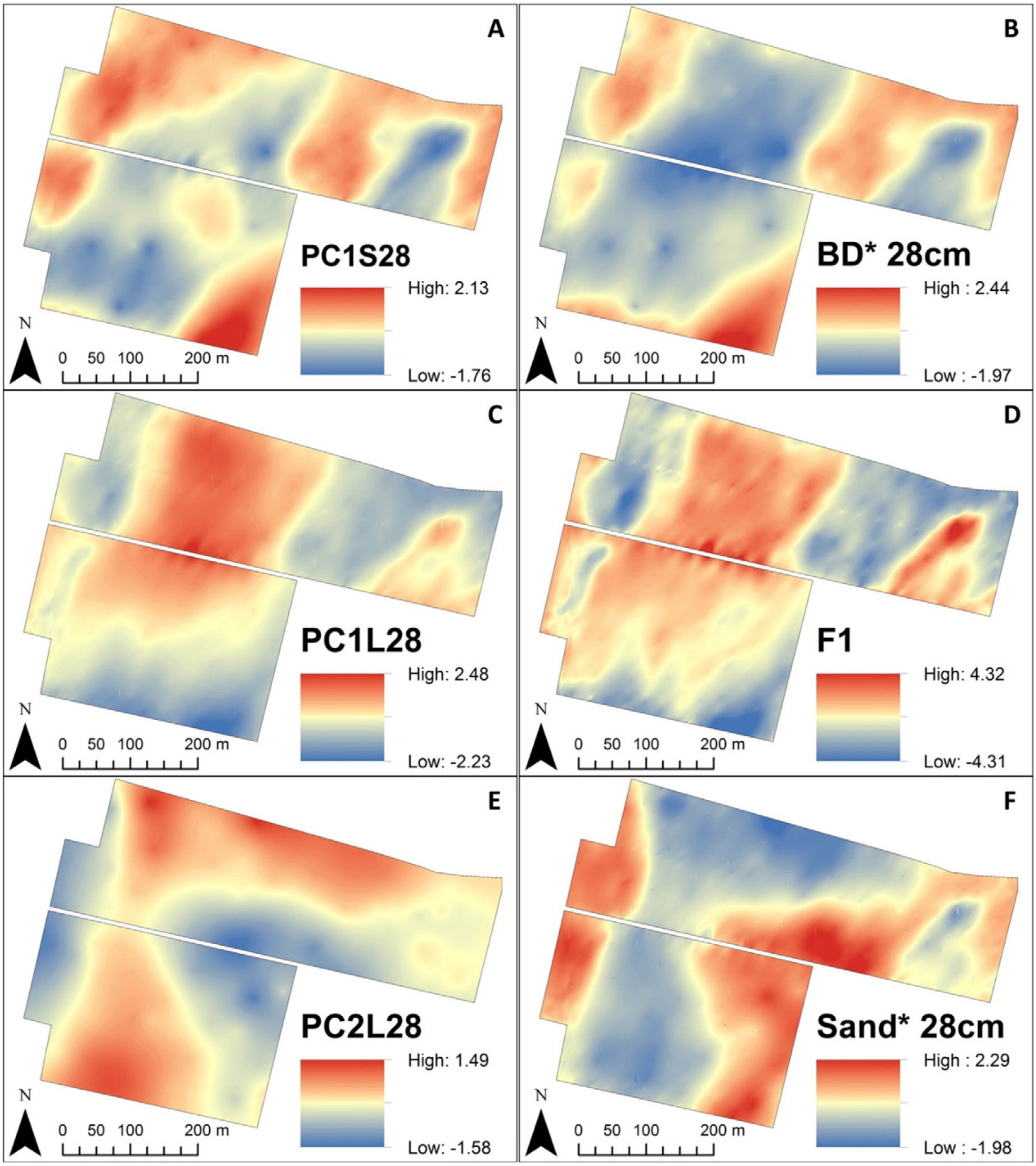

Fig. 5. Maps of retained PCs and their distribution counterparts at 28 cm depth. See the caption of Fig. 4 for the panel description and labeling.

explained between 34.5% and 5.6% of the variance. Of the second PCs, only the 28 cm long range was retained. The eigenvalues quantify the variance represented by each PC in absolute terms. Because they are absolute, we can use the ratio between eigenvalues for the first PC of long scale and short scale to identify which process is more dominant (Table 3). There is a strong trend between the L/S ratio and depth. At shallow depths, short scale processes are more dominant. As depth increases, long scale processes become more dominant. A second piece of supporting evidence comes from the strong linear trend ($R^2 = 0.92$) of decreasing sum of squared residuals (SSR) with depth. This makes sense because many short scale processes such as microbial activity, plant roots and others occur near the surface and not at depth.

At the short scale, PC1 (PC1SXX) is characterized by strong contributions from BD* and θ_s* (Table 10). α* and K_s* also tend to contribute to PC1SXX with α* loading slightly stronger than K_s*. This reflects the relative strengths in their relationships with BD*. It is not surprising that α* loads on the PC with BD* as one of the major differences between the curves in Fig. 3A is a lateral shift. Since there is a global trend and strong trends at this scale between K_s* and α*, it is also not surprising that K_s* loads too. As noted above, BD* appears to play a large role with K_s* than texture. In this case, texture does not really load and the loading strengths over all are weak. This makes inferences about a possible BD*, Sand* interaction impossible. In general, 68 cm deviates from the other layers at this scale.

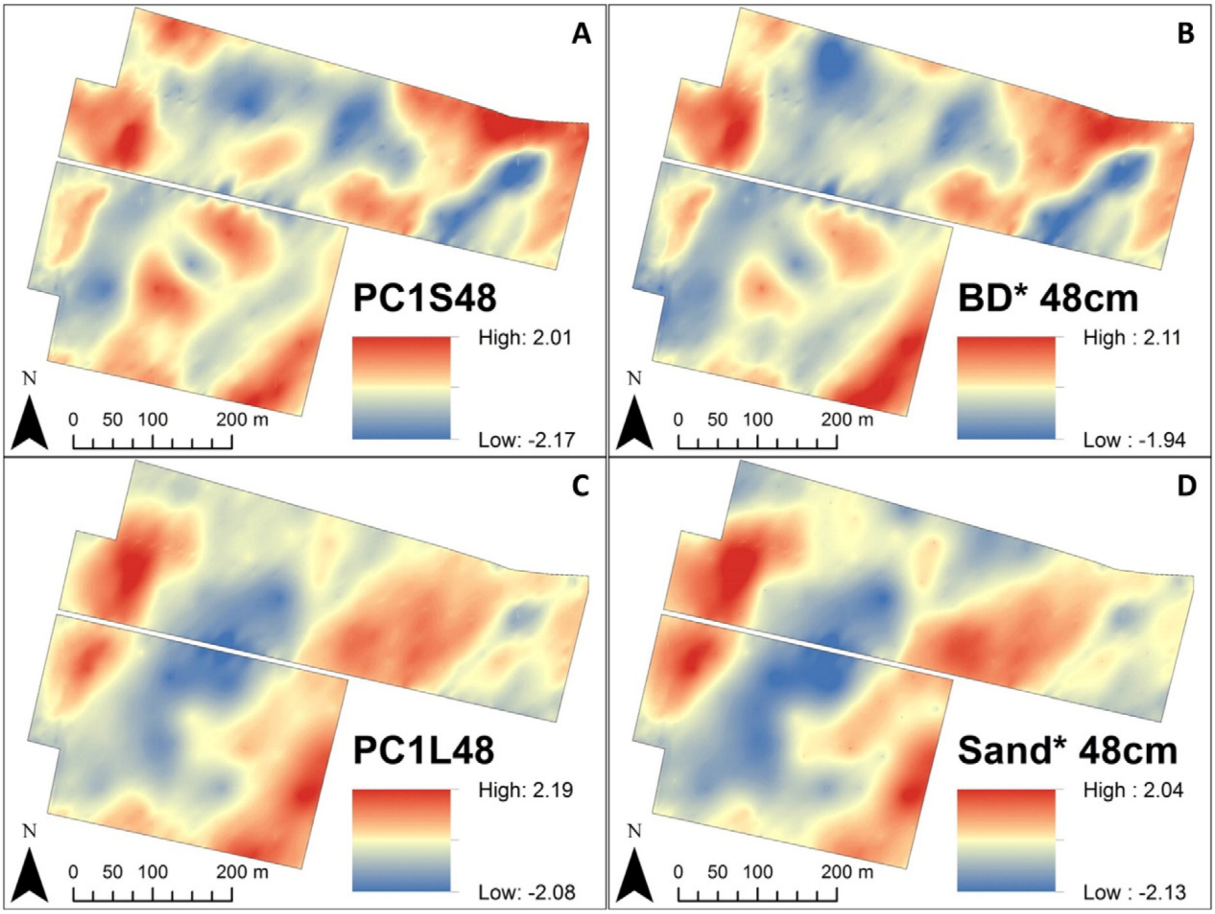

Fig. 6. Maps of retained PCs and their distribution counterparts at 48 cm depth. See the caption of Fig. 4 for the panel description and labeling.

At the long scale, PC1 (PC1LXX) is related to texture at all depths except 28 cm (Table 10). In general, 28 cm behaved differently than the other layers at this scale likely due to poor representation by the secondary variable (F1). 48 cm and 68 cm have similar behavior whereas 8 cm and 28 cm are more similar. At depths of 48 cm and 68 cm, n^* also contributes strongly on PC1L48 and PC1L68 respectively.

3.3.3. Spatial distribution of PCs

Spatial distributions of the retained PCs resemble the distributions of some of the studied variables as seen in Figs. 4–7. Contributions may be negative and therefore maps may be reciprocal yet have the same distribution. This is the case of PC1S08 with BD* or PC1L08 whith Elevation* (Fig. 4). PC1L28 is almost identical to F1, the secondary variable and PC2L28 resembles the distribution of Sand*, confirming the suspicion that F1 does not represent this layer well at long scale (Fig. 5).

At 48 cm (Fig. 6), the short scale PC1S48 map is identical to the map of BD* for this depth and long scale PC1L48 has a near identical match but to Sand* which resembles the shapes of the paleo-channels. The relationships at 68 cm (Fig. 7) are similar to those at 48 cm except a strong deviation in the southwest corner of PC1S68 from the distribution of BD*. Overall, the short scale distributions tend to visually resemble BD while the long scale distributions tend to visually resemble texture* and the paleo-channels.

4. Conclusions

The application of geostatistics to soil science has the potential to address some of the field most pressing issues. In particular, FKA is useful for identifying the underlying processes that affect the soil variables that are regularly studied. This type of analysis is effective at identifying relationships by removing scale dependency from the variables. When this is done, relationships become strong and more obvious. A subsequent variable reduction decreases the variable space into common factors which represent the related processes that act in the soil. Maps of these common factors can be used to identify the real world process. An issue of concern in unsaturated hydraulic research is that laboratory and field measurements often are not in agreement. This is likely caused by two sources of error, laboratory measurement errors and errors resulting from heterogeneity in the field.

This study assesses and demonstrates the use of FKA and related techniques to describe the heterogeneity of the field and identify how this heterogeneity affects the variables of interest. The originality of this study also relies on the application of the multivariate approach on a large dataset of unsaturated hydraulic parameters measured at different depths. The most significant finding is that physical variables and hydraulic variables both load on the same set of PCs. At short scale (less than 100 m), distributions tended to resemble bulk density while long scale (higher than 200 m) distributions resembled texture and the paleo-channel. This indicates that physical properties and hydraulic properties are linked to the same set of causal processes with the latter that can be estimated from the former. While this does not add value directly to the development of PTF, it does confirm that spatial application of PTF will likely find success. Also, using the spatial characteristics of the soil physical properties could be used to design a more efficient sampling scheme for soil hydraulic measurements.

This study suggests that there are many variables to considerer when investigating field versus lab error. For instance, depth is usually an under rated variable. We show that relationships between variables

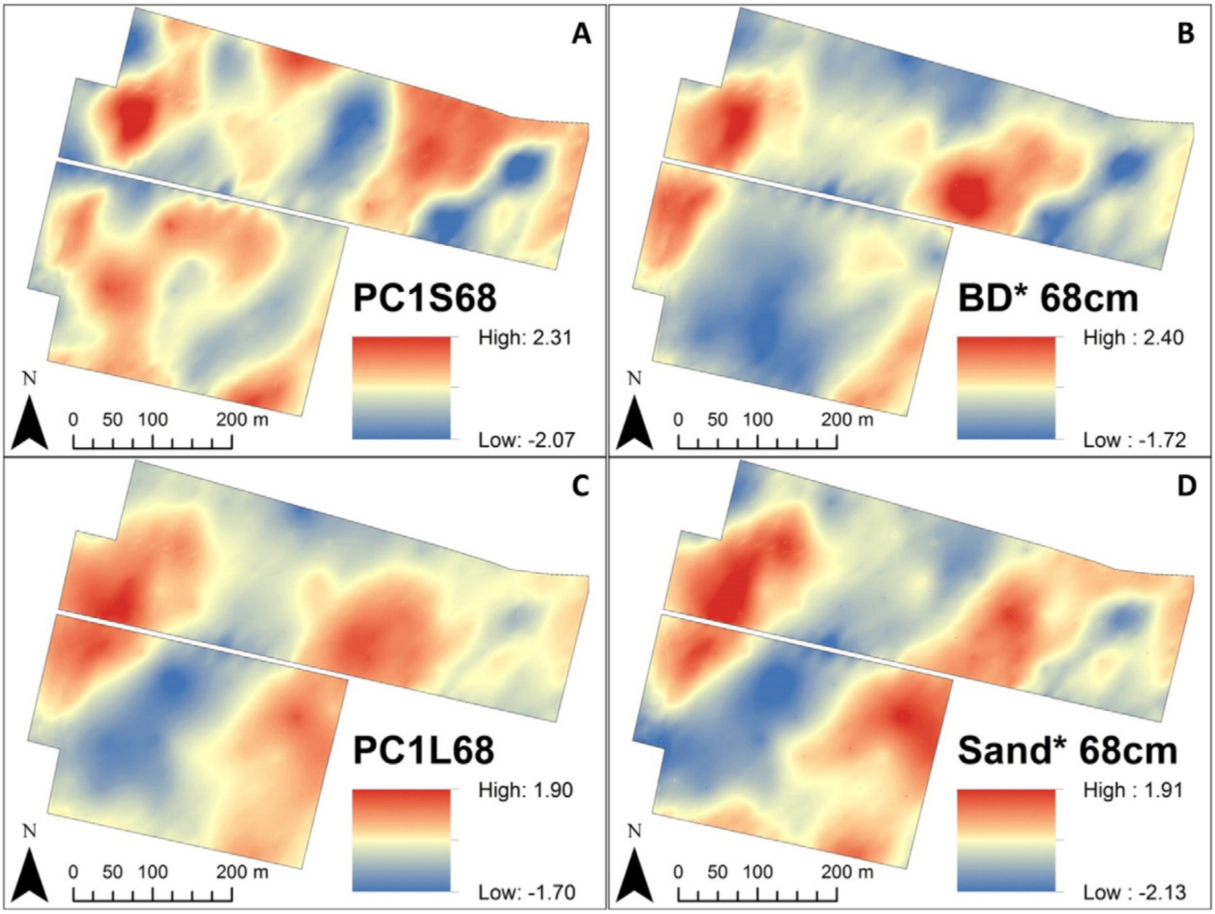

Fig. 7. Maps of retained PCs and their distribution counterparts at 68 cm depth. See the caption of Fig. 4 for the panel description and labeling.

change markedly along depth, with short scale processes that are more dominant than long scale processes closer the surface.

Considering the positive outcome of FKA, future studies will attempt to make zonal classification of hydraulic parameters from proximal and/or remotely sensed datasets to improve the application of advanced numerical models.

Acknowledgments

This study was funded within the Research Programme "GEO-RISKS: Geological, Morphological and Hydrological Processes: Monitoring, Modelling and Impact in the North-Eastern Italy", WP4, the University of Padova, Italy and by a grant from the United States Department of Agriculture — National Institute of Food and Agriculture — International Science and Education Program (Award No. 2010-51160-21050) to the TransAtlantic Precision Agriculture Consortium. The authors acknowledge the outstanding work of Dr. Gianluca Simonetti and Davide Piragnolo, who helped in the laboratory analyses.

Appendix A. Supplementary data

Supplementary data to this article can be found online at http://dx.doi.org/10.1016/j.geoderma.2015.08.025.

References

Alary, C., Demougeot-Renard, H., 2010. Factorial kriging analysis as a tool for explaining the complex spatial distribution of metals in sediments. Environ. Sci. Technol. 44, 593–599.

Biswas, B., Si, B., 2009. Spatial relationship between soil hydraulic and soil physical properties in a farm field. Can. J. Soil Sci. 89, 473–488.

Bocchi, S., Castrignanò, A., Fornaro, F., Maggiore, T., 2000. Application of factorial kriging for mapping soil variation at field scale. Eur. J. Agron. 13, 295–308.

Botros, F., Harter, T., Onsoy, Y., Tuli, A., Hopmans, J., 2009. Spatial variability of hydraulic properties and sediment characteristics in a deep alluvial unsaturated zone. Vadose Zone J. 8 (2), 276–289.

Castrignanò, A., Giugliarini, L., Risaliti, R., Martinelli, N., 2000. Study of spatial relationships among some soil physico-chemical properties of a field in central Italy using multivariate geostatistics. Geoderma 97, 39–60.

Chilés, J.P., Delfiner, P., 2012. Geostatistics: Modeling Spatial Uncertainty. 2nd ed. John Wiley & Sons, Inc., Hoboken, NJ.

Ciollaro, G., Romano, N., 1995. Spatial variability of the hydraulic properties of a volcanic soil. Geoderma 65, 263–282.

Corwin, D., Lesch, S., 2005. Apparent soil electrical conductivity measurements in agriculture. Comput. Electron. Agric. 46, 11–43.

Dane, T., Topp, G. (Eds.), 1994. SSSA Book Series: 5, Methods of Soil Analysis, Part 4 Physical Methods. Soil Science Society of America, Madison, WI.

Deurer, M., Duijnisveld, W., 2000. Spatial analysis of water characteristic functions in a sandy podzol under pine forest. Water Resour. Res. 36 (10), 2925–2935.

Dobermann, A., Goovaerts, P., George, T., 1995. Sources of soil variation in an acid Ultisol of Philippines. Geoderma 68, 173–191.

Doussan, C., Ruy, S., 2009. Prediction of unsaturated soil hydraulic conductivity with electrical conductivity. Water Resour. Res. 45, W10408. http://dx.doi.org/10.1029/2008WR007309.

Gambolati, G., Putti, M., Teatini, P., Gasparetto Stori, G., 2006. Subsidence due to peat oxidation and impact on drainage infrastructures in farmland catchment south of Venice Lagoon. Environ. Geol. 49, 814–820.

Goovaerts, P., 1992. Factorial kriging analysis: a useful tool for exploring the structure of multivariate spatial soil information. J. Soil Sci. 43, 597–619.

Goulard, M., Voltz, M., 1992. Geostatistical interpolation of curves: a case study in soil science. Geostat. Tróia 2, 805–816.

Greminger, P., Sud, Y., Nielsen, D., 1985. Spatial variability of field-measured soil–water characteristics. SSSAJ 49 (5), 1075–1082.

Groovaerts, P., 1998. Geostatistical tools for characterizing the spatial variability of microbiological and physico-chemical soil properties. Biol. Fertil. Soils 27, 315–334.

Hammel, K., Gross, J., Wessolek, G., Roth, K., 1999. Two-dimensional simulation of bromide transport in a heterogeneous field soil with transient unsaturated flow. Eur. J. Soil Sci. 50, 633–647.

Herbst, M., Diekkruger, B., Vereecken, H., 2006. Geostatistical co-regionalisation of soil hydraulic properties in a micro-scale catchment using terrain attributes. Geoderma 132, 206–221.
Jaynes, D., Tyler, E., 1984. Using soil physical properties to estimate hydraulic conductivity. Soil Sci. 138, 298–305.
Journel, A.G., Huijbregts, C.J., 1978. Mining Geostatistics. Academic Press, London, UK.
Li, Y., Chen, D., White, R.E., Zhu, A., Zhang, J., 2006. Estimating soil hydraulic properties of Fengqiu Country soils in the North China Plain using pedo-transfer functions. Geoderma 138, 261–271.
Loveland, P., Webb, J., 2003. Is there a critical level of organic matter in the agricultural soils of temperate regions: a review. Soil Tillage Res. 70, 1–18.
Mallants, D., Binayak, M., Diederik, J., Feyen, J., 1996. Spatial variability of hydraulic properties in a multi-layered soil profile. Soil Sci. 161 (3), 167–181.
Mallants, D., Tseng, P., Toride, N., Timmerman, A., Feyen, J., 1997a. Evaluation of multimodal hydraulic functions in characterizing a heterogeneous field soil. J. Hydrol. 195, 172–199.
Mallants, D., Mohanty, B., Vervoot, A., Feyen, J., 1997b. Spatial analysis of saturated hydraulic conductivity in a soil with macropores. Soil Technol. 10, 115–131.
Mertens, J., Jacques, D., Vanderborght, J., Feyen, J., 2002. Characterisation of the field-saturated hydraulic conductivity on a hillslope: in situ single ring pressure infiltrometer measurements. J. Hydrol. 263, 217–229.
Mualem, Y., 1976. A new model for predicting the hydraulic conductivity of unsaturated conductivity of unsaturated porous media. Water Resour. Res. 12 (3), 513–522.
Nanos, N., Martín, J., 2012. Multiscale analysis of heavy metal contents in soils: spatial variability in Duero river basin (Spain). Geoderma 189–190, 554–562.
Pachepsky, Y.A., Rawls, W.J., Lin, H.S., 2006. Hydropedology and pedotransfer functions. Geoderma 131, 308–316.
Puckett, W., Dane, J., Hajek, B., 1985. Physical and mineralogical data to determine soil hydraulic properties. Soil Sci. Soc. Am. J. 49, 831–836.
Radcliffe, D., Simunek, J., 2010. Soil Physics With HYDRUS: Modeling and Applications. Taylor and Francis Group, Boca Raton, FL.
Rouse, J., Haas, R., Schell, J., Deering, D., 1973. Monitoring vegetation systems in the Great Plains with ERTS. Third ERTS Symposium. NASA SP-351, pp. 309–317.
Russo, D., Jury, W., 1987. A theoretical study of the estimation of correlation scale in spatially variable fields 1. Stationary fields. Water Resour. Res. 23 (7), 1257–1268.
Saito, H., Seki, K., Simunek, J., 2009. An alternative deterministic method for the spatial interpolation of water retention parameters. Hydrol. Earth Syst. Sci. 13, 453–465.
Schaap, M., Bouten, W., 1996. Modeling water retention curves of sandy soils using neural networks. Water Resour. Res. 32 (10), 3033–3040.
Schaap, M., Leij, F., 2000. Improved prediction of unsaturated hydraulic conductivity with the Mualem–van Genuchten model. SSSAJ 64, 843–851.
Scudiero, E., Deiana, R., Teatini, P., Cassiani, G., Morari, F., 2011. Constrained optimization of spatial sampling in salt contaminated coastal farmland using EMI and continuous simulated annealing. Procedia Environ. Sci. 7, 234–239.
Scudiero, E., Teatini, P., Corwin, D., Berti, A., Deiana, R., Morari, F., 2013. Delineation of site-specific management units in a saline region at the Venice Lagoon margin, Italy, using soil reflectance and apparent electrical conductivity. Comput. Electron. Agric. 99, 54–64.
Simunek, J., Sejna, M., Saito, H., Sakai, M., van Genuchten, M.Th., 2008. The HYDRUS-1D Software Package for Simulating the One-dimensional Movement of Water, Heat, and Multiple Solutes in Variably-saturated Media, Version 4.0x, Hydrus Series 3. Department of Environmental Sciences, University of California Riverside, Riverside, CA, USA.
Soil Survey Staff, 1998. Keys to Soil Taxonomy (eighth ed.). USDA–NRCS, Washington, DC.
Sollitto, D., Romic, M., Castrignanò, A., Romic, D., Bakic, H., 2010. Assessing heavy metal contamination in soils of Zagreb region (Northwest Croatia) using multivariate geostatistics. Catena 80, 182–194.
Ünlü, K., Nielsen, D., Biggar, J., Morkoc, F., 1990. Statistical parameters characterizing the spatial variability of selected soil hydraulic properties. SSSAJ 54, 1537–1547.
van Genuchten, M., 1980. A closed-form equation for predicting the hydraulic conductivity of unsaturated soil. Soil Sci. Soc. Am. J. 44 (5), 892–898.
Vauclin, M., Elrick, D., Thony, J., Vachaud, G., Revol, Ph., Ruelle, P., 1994. Hydraulic conductivity measurements of the spatial variability of a loamy soil. Soil Technol. 7, 181–195.
Vereecken, H., Weynants, M., Javaux, M., Pachepsky, Y., Schaap, M.G., van Genuchten, M.Th., 2010. Using pedotransfer functions to estimate the van Genuchten–Mualem soil hydraulic properties: a review. Vadose Zone J. 9, 795–820.
Voltz, M., Goulard, M., 1994. Spatial interpolation of soil moisture retention curves. Geoderma 62, 109–123.
Wackernagel, H., 2003. Multivariate Geostatistics. 3rd ed. Springer-Verlag, Berlin, Heidelberg, Germany.
Walczak, R., Rovdan, E., Witkowska-Walczak, B., 2002. Water retention characteristics of peat and sand mixtures. Int. Agrophys. 16, 161–165.
Weynants, M., Vereecken, H., Javaux, M., 2009. Revisiting Vereecken pedo transfer functions: introducing a closed-form hydraulic model. Vadose Zone J. 8, 86–95.
Wierenga, P., Hills, R., Hudson, D., 1991. The Las Cruces Trench Site: characterization, experimental results, and one-dimensional flow predictions. Water Resour. Res. 27 (10), 2695–2705.
Wösten, J., Pachepsky, Ya., Rawls, W., 2001. Pedotransfer functions: bridging the gap between available basic soil data and missing soil hydraulic characteristics. J. Hydrol. 251, 123–150.
Zimmermann, A., Schinn, D., Francke, T., Elsenbeer, H., Zimmermann, B., 2013. Uncovering patterns of near-surface saturated hydraulic conductivity in an overland flow-controlled landscape. Geoderma 196, 1–11.